EMPIRICAL EVIDENCE AND STABILITY ANALYSIS OF THE LINEAR CAR-FOLLOWING MODEL WITH GAMMA-DISTRIBUTED MEMORY EFFECT

Authors

Xin PEI*

Department of Automation, Tsinghua University, Beijing, China

Tel: (86) 10 6279 5043

Fax: (86) 10 6279 5043

Email: peixin@mail.tsinghua.edu.cn

Yan PAN

Department of Automation, Tsinghua University, Beijing, China

Email: pany11@mails.tsinghua.edu.cn

Haixin WANG

Department of Civil Engineering, The University of Hong Kong, Hong Kong, China

Email: wanghaixin90@126.com

S.C. WONG

Department of Civil Engineering, The University of Hong Kong, Hong Kong, China

Email: hhecwsc@hku.hk

Keechoo CHOI

Department of Transportation Engineering, TOD-based Sustainable Urban Transportation, Center, Ajou University, Republic of Korea

E-mail: keechoo@ajou.ac.kr

ABSTRACT

Car-following models, which describe the reactions of the driver of a following car to the changes of the leading car, are essential for the development of traffic flow theory. A car-following model with a stochastic memory effect is considered to be more realistic in modeling drivers' behavior. Because a gamma-distributed memory function has been shown to outperform other forms according to empirical data, in this study, we thus focus on a car-following model with a gamma-distributed memory effect; analytical and numerical studies are then conducted for stability analysis. Accordingly, the general expression of undamped and stability points is achieved by analytical study. The numerical results show great agreement with the analytical results: introducing the effect of the driver's memory causes the stable regions to weaken slightly, but the metastable region is obviously enlarged. In addition, a numerical study is performed to further analyze the variation of the stable and unstable regions with respect to the different profiles of gamma distribution.

Keywords:

Car-following model; memory effect; gamma distribution; stability analysis; empirical study

1 INTRODUCTION

Car-following models, which describe the following driver’s reaction to the changes of the leading car, are essential for the development of traffic flow theory. Such models build a bridge between the microscopic behavior of the following driver and the macroscopic characteristics of the traffic flow by analysis of the responses of each following vehicle in a single-lane car-following system.

In the 1950s, Chandler et al. (1958) and Herman et al. (1959) proposed a mathematical car-following model in which it is assumed that the acceleration of the following car in each two-vehicle unit is linearly proportional to the cars’ relative velocities at some earlier time, with a fixed time lag of transmission of the driver-vehicle system. Herman et al. (1959) also provided a systematic discussion of the stability. The results accounted for the local stability and corresponding numerical calculations, and also for the asymptotic stability, car-following control, and acceleration noise. In addition to the linear car-following model, Reuschel (1950), Pipes (1953), Gazis et al. (1961), and Newell (1961) developed various nonlinear models in which other variables are included that may affect the behavior of the following driver.

In recent decades, improved car-following models have been proposed to better explain the behavior of drivers and the stability of the traffic flow. Bando et al. (1995) proposed an optimal velocity model to represent the instability of traffic flow and the evolution of congestion. Jiang et al. (2001) developed a full velocity difference model by differentiation of the deceleration and acceleration processes. Ge et al. (2012) extended the car-following model to consider the effects of a series of leading vehicles. In concern of memory effect of time-series variations, the traditional model is developed by incorporating the driver’s memory of speeds at or during a certain time ahead (Zhang, 2003; Tang et al. 2009; Xin and Xu, 2015). Treiber and Helbing (2003) concerned memory effect of the subjective level of service dependent on speed, which represents the adaptation of drivers to the surrounding traffic situation during past few minutes, for macroscopic modeling of flow-density data. Yu and Shi (2015a) adopted empirical data to improve the car-following model by including memory of headway changes, which was further concerned in cooperative adaptive cruise control strategy (Yu and Shi, 2015b). Cao (2015) also considered the memory effect of headway during a sensory time period during a certain past time. In consideration of the forecast information attributable to ITS techniques, Tang et al. (2010) involved driver's forecast effect in car-following model. More recently, with the development of connected vehicles, an improved car-following model with delayed acceleration reaction is proposed (Jin and Orosz, 2014). Ngoduy (2013, 2015) and Monteil et al. (2014) further focus on the stability of traffic flow in concern of car-following model in a simulated connected vehicle framework.

The time lag, which is related to reaction time, is of great concern in previous studies on macroscopic and microscopic traffic models (Treiber et al., 2006; Kesting and Treiber, 2008). Generally speaking, the existing car-following models always consider the time lag as a fixed parameter that is estimated in terms of the average or optimal values on the basis of realistic traffic information, even in most memory effect related research mentioned previously. However, in practice, the reactions of the following driver are affected not only by the motion of the vehicles at a certain earlier instant, but also by continuous motions during an earlier period, which can be reflected in the driver's memory, i.e., a memory effect. Classic studies have focused on the memory effects of drivers in the car-following process. Based on the work of Chandler et al. (1958) and Herman et al. (1959), Lee (1966) introduced the function of memory into the traditional car-following model to define the manner in which the following driver processes the information received from the leading car by means of the memory effect. The proposed memory effect model is considered to be more realistic in modeling drivers' behavior.

As shown in Lee's study, the acceleration of the following car is influenced only by the relative speeds. The difference here is that the reactions of the following car are not determined by the relative speeds at a certain earlier instant, but rather by the time history. The memory function is added to the model by the introduction of a stochastic time lag, which may follow a particular distribution over time. Lee (1966) described the memory effect with several possible memory functions in his study, such as a Dirac-Delta function (with which the model is reduced to a traditional one), a decaying exponential function (which is also a special case of the gamma-distributed function), another special gamma-distributed function with a concave curve, and a uniform-distributed function. Relevant stability analysis of the local stability and asymptotic stability were also performed in his study. Unfortunately, without experimental data, the advantage of the memory effect model is difficult to assess, although it is considered to be a more realistic means by which to describe the following driver's behavior. In addition, the optimal form of memory function could not be determined. Sipahi et al. (2007) have conducted the stability analysis of car-following system with gamma distributed time lag. However, they did not validate the superior performance of gamma distribution, and did not achieve the analytical solution of critical points in local stability analysis.

In this study, we attempt to reveal the most appropriate distribution for memory effect with empirical data. Analytical and numerical studies are then conducted for stability analysis, and the general expression of undamped and stability points is achieved by analytical study, accordingly. A numerical study is performed to further analyze the variation of the stable and unstable regions with respect to the different profiles of memory effect.

The remainder of this paper is organized as follows. In section 2, after the introduction of the model formulation, several distribution forms of memory effect are proposed. Based on empirical data collected from car-following field experiments, the optimal form of memory effect is obtained. In section 3, an analytical study of the local stability is conducted to explore the demarcations between stability and instability and between damped oscillation and amplifying oscillation. In section 4, a numerical study is carried out to show agreement with the analytical results. Section 5 presents the concluding remarks and recommendations for future research.

2 PRELIMINARY STUDY AND EMPIRICAL ANALYSIS

2.1 Model Formulation

According to the study of Chandler et al. (1958), each of the cars in a line of traffic follows the preceding car by means of velocity control. This control equation of motion is

$$M\frac{d^2x_{n+1}}{dt^2}=\lambda\left(\frac{dx_n}{dt}-\frac{dx_{n+1}}{dt}\right)_{t-\Delta}, \qquad \text{2-1}$$

where M and λ are the mass and sensitivity of each car, respectively, x_n is the location of the *n*th vehicle in the line, and Δ is the time lag of transmission of the driver-vehicle system.

Simplifying Equation (2-1) to

$$\ddot{x}_{n+1}(t)=\alpha(\dot{x}_n(t-\Delta t)-\dot{x}_{n+1}(t-\Delta t)), \qquad \text{2-2}$$

where $\alpha=\lambda/M$, denotes the sensitivity of the entire driver-vehicle system, $\ddot{x}_{n+1}(t)$ is the acceleration of the $(n+1)$th car at time *t*, and $\dot{x}_n(t-\Delta t)$ and $\dot{x}_{n+1}(t-\Delta t)$ are the velocities of the *n*th and $(n+1)$th cars at time $(t-\Delta t)$. Obviously, Δt is the time lag.

Equation (2-2) shows that the acceleration of the following vehicle at time *t* is determined by the difference in the velocities of the lead and following vehicles at time $(t-\Delta t)$, with a sensitivity α. We notice that the reactions of the following driver are affected only by the relative velocities at a certain earlier instant $(t-\Delta t)$. The information regarding other previous moments has been neglected, even though some of this information would have a small effect in determining the current acceleration of the following vehicle. This information does make a contribution and will distract the weight of the differences in the velocities at a particular time. Therefore, a nonconstant time lag is incorporated into the traditional car-following model to describe the driver’s memory effect and to simulate the memory-choice-decision process.

As in Lee's model, the improved car-following model with memory effect is formulated on the basis of Equation (2-2) as:

$$\ddot{x}_{n+1}(t) = \alpha \int_0^{+\infty} f(\omega)(\dot{x}_n(t-\omega) - \dot{x}_{n+1}(t-\omega))d\omega, \tag{2-3}$$

where $\omega(\geq 0)$ is the stochastic time lag with a memory function of $f(\omega)$.

Lee (1966) adopted several possible memory functions to describe $f(\omega)$ in his study, such as a Dirac-Delta function (with which the model is reduced to a traditional one), a decaying exponential function (which is also a special case of the gamma-distributed function), another special gamma-distributed function with a concave curve, and a uniform-distributed function. In addition to the four examples of memory function, alternative memory functions can further be considered with regard to the characteristics of the human memory. We believe that the probability density function that can properly describe the driver's memory effect should be a curve over time, an approximately concave curve with a point that occupies the greatest probability as the average or most probable value of the time lag in the traditional car-following model. When the time lag exceeds that point, the information regarding the relative velocity is less important and the driver's dependence on it will decrease. That is, the driver needs not be concerned about the information stored in his mind from a long time ago. When the time lag does not reach that point, the information becomes even more important; however, the driver does not have sufficient time to think and to react accordingly. The closer the time lag approaches the current time, the more difficult it is for the driver to react. Hence, the curve of the probability density function should monotonically increase up to the peak that dominates in the past information and then declines, forward to infinity with a probability that approaches zero. Accordingly, several classical distributions, such as gamma distribution, Weibull distribution, and lognormal distribution, can also be considered for memory function formulation.

Taking gamma-distributed memory function as an example, $\omega \sim \Gamma(k, \lambda)$, and $f(\omega)$ should be the probability density functions of the gamma distribution with parameters k, λ. Thus,

$$f(\omega) = \frac{\lambda^k \omega^{k-1} e^{-\lambda\omega}}{\Gamma(k)}$$
$$\Gamma(k) = \int_0^{\infty} x^{k-1} e^{-x} dx \tag{2-4}$$

where $\omega \geq 0,\ \lambda \geq 0,\ k \geq 0$,. The mean and variance of the distribution are $\frac{k}{\lambda}$ and $\frac{k}{\lambda^2}$, respectively.

The car-following model with a memory effect states that the $(n+1)$th vehicle's acceleration at t is determined by the relative velocities at $t - \omega$, the sensitivity, and the function of ω. The driver's memory effect is taken into account in terms of the integral term.

2.2 Empirical study of memory function

To identify the optimal form of memory function, we conducted empirical car-following experiments in which four drivers were asked to follow a leading car for four trials. The average age of drivers are 41 with S.D. of 20, and the average driving age is 15 with S.D. of 14. The experiments were conducted at the 1st Yuanbo West Rd in Beijing, China on Nov. 22, 2014. The survey road is a 4-lane rural road of 1.2 km length with central divider. There was no other traffic during experiments. The leading car travelled automatically with a preset speed profile: keeping 45 km/h during the first 4 s, followed by a sinuous variation between 30-60 km/h. The following car controlled by the driver just followed the leading car. **Fig. 1** illustrates the speed profile of the leading car (speed 1) and following car (speed 2) during trial 1 by Driver #1. During the experiments, the velocity, acceleration, location of both cars were recorded every 0.2 s.

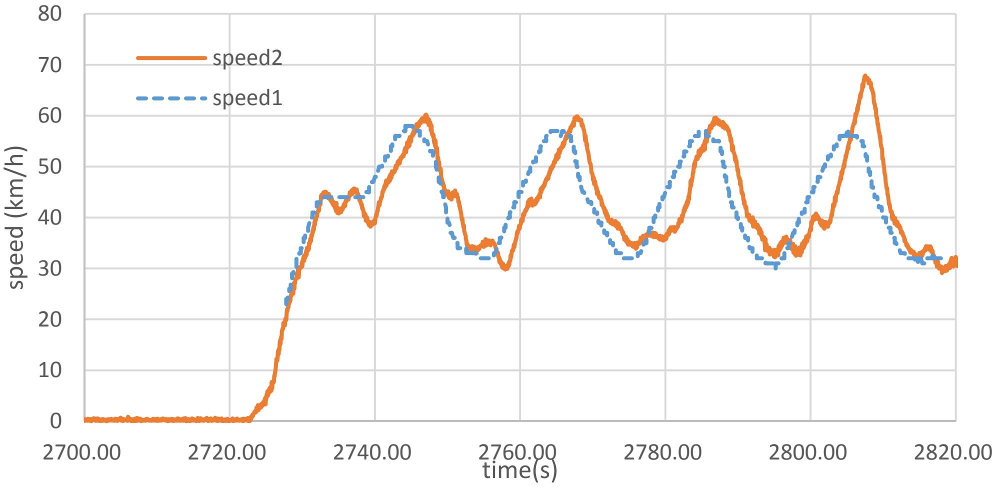

Fig. 1. Speed profiles of the leading car (speed 1) and following car (speed 2) during trial 1-1

On the basis of the experimental data, the acceleration of the following car can be predicted by the traditional car-following model, and the improved memory effect models with a memory function based on uniform distribution, gamma distribution, Weibull distribution, and lognormal distribution, respectively. A RMSE (Root Mean Squared Error) based goodness-of-fit test is adopted for model calibration. The lower the value of RMSE, the better the goodness-of-fit of proposed model. The corresponding RMSE values of each trial among 5 different models are shown in Table 1. The lowest RMSE value for each trial among all of the models is expressed in bold font.

Table 1. RMSE Comparison of memory effect models with traditional one

Driver-Trial	Traditional model	Memory effect model with different memory function			
		Gamma	Lognormal	Weibull	Uniform
1-1	0.5708	**0.5691**	**0.5691**	0.5694	0.5695
1-2	0.8516	**0.8492**	**0.8492**	0.8499	0.8494
1-3	0.6649	0.6329	**0.6310**	0.6344	0.6374
1-4	0.7481	0.7379	**0.7292**	0.7413	0.7405
2-1	0.4451	**0.4444**	**0.4444**	0.4447	**0.4444**
2-2	0.3738	**0.3728**	0.3730	0.3729	0.3731
2-3	0.4798	**0.4766**	0.4767	0.4767	0.4767
2-4	0.4190	**0.4180**	**0.4180**	**0.4180**	0.4184
3-1	0.4323	**0.4288**	**0.4288**	0.4294	0.4289
3-2	0.4587	**0.4579**	0.4587	0.4580	0.4580

Driver-Trial	Traditional model	Memory effect model with different memory function			
		Gamma	Lognormal	Weibull	Uniform
3-3	0.3349	**0.3297**	**0.3297**	0.3303	0.3298
3-4	0.4070	0.4051	0.4051	0.4051	**0.4050**
4-1	0.3352	0.3147	0.3133	0.3135	**0.3129**
4-2	0.3571	**0.3532**	**0.3532**	0.3535	0.3536
4-3	0.3478	**0.3438**	**0.3438**	0.3440	0.3439
4-4	0.3816	**0.3770**	**0.3770**	0.3776	0.3773

As shown in the result, the improved car-following model with a memory effect performs better than the traditional model in all 16 trials. In addition, the gamma-distributed memory function generally performs better in all of trials. Therefore, in the following discussion, we focus on the gamma-distributed memory function and its stability, especially the local stability. This is important to understand the memory effect on car-following behavior and traffic conditions, which has rarely been studied in the literature.

3 ANALYTICAL STUDY

3.1 Laplace transform

Assume that before $t = 0$ each vehicle moves with a speed u. Using a locally moving coordinate representation,

$$z_n(t) = x_n(t) - ut - x_n(0). \qquad \text{3-1}$$

Obviously, when $t \leq 0$， $z_n(t) = 0$， $\dot{z}_n(t) = 0$, the Equation (2‒3) can be rewritten as the following formula according to the convolution theorem,

$$\begin{aligned} \ddot{z}_{n+1}(t) &= \alpha \int_0^t f(\omega)(\dot{z}_n(t-\omega) - \dot{z}_{n+1}(t-\omega))d\omega \\ &= \alpha \cdot f(t) * \left(\dot{z}_n(t) - \dot{z}_{n+1}(t)\right). \end{aligned} \qquad \text{3-2}$$

Meanwhile, we define the Laplace transform of $z_n(t)$ as

$$Z_n(s) = L\left(z_n(s)\right) = \int_0^\infty z_n(t) e^{-st} dt. \qquad \text{3-3}$$

Therefore,

$$L\left(\ddot{z}_n(t)\right) = s^2 Z_n(s) - s z_n(0) - \dot{z}_n(0) = s^2 Z_n(s), \qquad \text{3-4}$$

$$L\big(\dot{z}_n(t)\big) = sZ_n(s) - z_n(0) = sZ_n(s) \ .$$

We then take the Laplace transform on both sides of Equation (2-3),

$$s^2 Z_{n+1}(s) = \alpha \cdot F(s) \cdot \big(sZ_n(s) - sZ_{n+1}(s)\big) \,, \tag{3-5}$$

$$Z_{n+1}(s) = \frac{\alpha \cdot F(s)}{s + \alpha \cdot F(s)} Z_n(s), \tag{3-6}$$

where $F(s)$ is the Laplace transform of $f(\omega)$. We may easily determine via MATLAB that

$$F(s) = \frac{\lambda^k}{(\lambda + s)^k} \ . \tag{3-7}$$

Therefore, we can obtain the transfer function for stability analysis as

$$\begin{aligned} Z_{n+1}(s) &= \frac{\alpha \lambda^k}{s(\lambda + s)^k + \alpha \lambda^k} Z_n(s) \\ &= \frac{\alpha^n \lambda^{kn}}{(s(\lambda + s)^k + \alpha \lambda^k)^n} Z_1(s). \end{aligned} \tag{3-8}$$

3.2 Undamped point

The undamped point is the demarcation between damped oscillation and amplifying oscillation, which is measured by $C = \alpha \Delta \mathrm{t}$, i.e., the sensitivity multiplied by the time lag. Because the time lag is not constant in this study, we use the mean of the gamma-distributed time lag k/λ instead. Thus, $C = \alpha \frac{k}{\lambda}$. The undamped point is an important index. If the computational value exceeds that point, it is fairly dangerous because the spacing change between the two vehicles is unstable and will never tend toward stability, which may result in a collision. On the basis of this undamped point, we can control some of the parameters in the car-following system to avoid any accidents.

According to Equation (3-8), which is the transfer function of the improved car-following model with a gamma-distributed memory effect, we discuss the properties of the possible solutions according to the characteristic roots of the following equation

$$s(\lambda + s)^k + \alpha \lambda^k = 0. \tag{3-9}$$

Although k can be any positive value in a gamma distribution, we assume that k is an integer, i.e., with an accuracy of 1, for further derivations, which has been accepted in practice by the previous empirical analysis and the following numerical study.

Because the profiles of the gamma distributions of $k = 1$ and $k > 1$ and the corresponding stability solutions are completely different, the following discussion is be presented separately.

When $k = 1$, then

$$s^2 + \lambda s + \alpha\lambda = 0. \tag{3-10}$$

Because $\lambda \geq 0, \alpha \geq 0$, the roots of Equation (3-10) always have negative real parts. This implies that regardless of the value of C, the spacing is either non-oscillatory or oscillatory with a decreasing amplitude.

We then turn to $k > 1$. Assuming that $y = \frac{\lambda+s}{\lambda} = 1 + \frac{s}{\lambda}$, then $s = \lambda y - \lambda$. Accordingly, Equation (3-9) should be rewritten as

$$\lambda y^{k+1} - \lambda y^k + \alpha = 0. \tag{3-11}$$

Let $c = \frac{\alpha}{\lambda}$, then $C = \alpha\frac{k}{\lambda} = ck$, thus

$$y^{k+1} - y^k + c = 0. \tag{3-12}$$

Let $y = te^{\theta i} = t \cdot \cos\theta + i \cdot t \cdot \sin\theta$, where $t > 0$, $0 < \theta \leq 2\pi$, $k \geq 2$, then

$$s = \lambda(t \cdot \cos\theta - 1 + i \cdot t \cdot \sin\theta). \tag{3-13}$$

Equation (3-12) is rewritten as

$$t^k(te^{(k+1)\theta i} - e^{k\theta i}) + c = 0. \tag{3-14}$$

Moreover，

$$c = -t^k\left[t \cdot \cos\big((k+1)\theta\big) + i \cdot t \cdot \sin\big((k+1)\theta\big) - \cos(k\theta) - i \cdot \sin(k\theta)\right]. \tag{3-15}$$

It is then equal to two equations,

$$t \cdot sin\big((k+1)\theta\big) - sin(k\theta) = 0,$$
$$t^k[t \cdot cos\big((k+1)\theta\big) - cos(k\theta)] + c = 0. \qquad \text{3-16}$$

As for the undamped point, let $t \cdot \cos\theta = 1$; we then have

$$\begin{cases} (1/\cos\theta) \cdot \sin\big((k+1)\theta\big) - \sin(k\theta) = 0 \\ c = -t^k[t \cdot \cos\big((k+1)\theta\big) - \cos(k\theta)] \end{cases} \Rightarrow \begin{cases} \cos(k\theta) \cdot \sin\ \theta = 0 \\ c = \dfrac{\sin(k\theta) \cdot \sin\theta}{(\cos\theta)^{k+1}} \end{cases}. \qquad \text{3-17}$$

If $\sin\theta = 0$, then $c = 0$, and $C = 0$. According to Equation (3-13), *s* is then a real number. Because of Descartes' rule of signs, there are no positive real roots for Equation (3-9). Therefore, *s* must be negative, and the spacing is non-oscillatory.

If $\cos(k\theta) = 0$, namely,

$$k\theta = \frac{\pi}{2},\ \ \frac{3\pi}{2},\ \ \frac{5\pi}{2} \ldots \qquad \text{3-18}$$

When $k = 2$,

$$\theta = \frac{\pi}{4},\ \ \frac{3\pi}{4},\ \ \frac{5\pi}{4} \ldots$$
$$c = 2\,,$$
$$C = ck = 4.$$

When $k = 3$,

$$\theta = \frac{\pi}{6},\ \ \frac{3\pi}{6},\ \ \frac{5\pi}{6} \ldots$$
$$c = 8/9\,,$$
$$C = ck = 8/3.$$

When $k \to \infty$,

$$\lim_{k\to\infty} C = \lim_{k\to\infty} k * \frac{\sin(k\theta)\cdot\sin\theta}{(\cos\theta)^{k+1}} = \lim_{k\to\infty} k * \sin\left({}^{\pi}\!/_{2k}\right) = \frac{\pi}{2},$$

which is consistent with the demarcation between damping and amplification as identified by Herman et al. (1959).

As a result,

a) If $C < k * \frac{\sin(k\theta)\cdot\sin\theta}{(\cos\theta)^{k+1}}$, the spacing is non-oscillatory, or oscillatory with damped oscillation;

b) if $C = k * \frac{\sin(k\theta)\cdot\sin\theta}{(\cos\theta)^{k+1}}$, the spacing is oscillatory with undamped oscillation; and

c) if $C > k * \frac{\sin(k\theta)\cdot\sin\theta}{(\cos\theta)^{k+1}}$, the spacing is oscillatory with an increasing amplitude, where θ is given by Equation (3-18).

3.3 Stability point

The stability point is the demarcation between oscillation and stability, which is also measured by $C = \alpha\frac{k}{\lambda}$. Likewise, we take Equation (3-9) for consideration. Identification of the dominant root is essential for the demarcation of oscillation and stability.

We assume that

$$f(s) = s(\lambda + s)^k + \alpha\lambda^k. \tag{3-19}$$

We then explore the curve profile of $f(s)$ based on its monotonic feature, from which the characteristic roots and corresponding stability can be inferred.

The derivative of $f(s)$ is

$$\begin{aligned} f'(s) &= (\lambda + s)^k + sk(\lambda + s)^{k-1} = (\lambda + s)^{k-1}(\lambda + s + sk) \\ &= (\lambda + s)^{k-1}((k+1)s + \lambda) \end{aligned} \tag{3-20}$$

When $f'(s) = 0$, the extreme points are

$$s = -\lambda, \tag{3-21}$$

and

$$s = -\frac{\lambda}{k+1}. \tag{3-22}$$

The second derivative of $f(s)$ is

$$\begin{aligned} f''(s) &= (k-1)(\lambda + s)^{k-2}\big((k+1)s + \lambda\big) + (\lambda + s)^{k-1}(k+1) \\ &= (\lambda + s)^{k-2}\big((k^2-1)s + \lambda(k-1) + \lambda k + \lambda + sk + s\big) \\ &= (\lambda + s)^{k-2}((k^2+k)s + 2\lambda k) \end{aligned} \tag{3-23}$$

Substituted by the root of extreme points, it becomes

$$f''(-\lambda) = 0, \text{ and} \tag{3-24}$$

$$f''\left(-\frac{\lambda}{k+1}\right) = \left(\frac{k\lambda}{k+1}\right)^{k-2}(-k\lambda + 2\lambda k) = \left(\frac{k\lambda}{k+1}\right)^{k-2}\lambda k > 0. \qquad 3\text{-}25$$

The extreme points are then given by

$$f\left(-\frac{\lambda}{k+1}\right) = -\frac{\lambda}{k+1}\left(\frac{k\lambda}{k+1}\right)^{k} + \alpha\lambda^{k} = \lambda^{k}\left(\alpha - \frac{k^{k}}{(k+1)^{k+1}}\lambda\right), \text{ and} \qquad 3\text{-}26$$

$$f(-\lambda) = \alpha\lambda^{k} > 0. \qquad 3\text{-}27$$

which accidentally equals $f(0)$.

According to Equation (3-26), when $s = -\frac{\lambda}{k+1}$, the function of $f(s)$ is convex in the near region, in which it reaches its local minimum.

For $s < -\lambda$, the monotonic feature of $f(s)$ is related to

$$f'(s) = (\lambda + s)^{k-1}((k+1)s + \lambda). \qquad 3\text{-}28$$

Because the sign of $(\lambda + s)^{k-1}$ is determined by the parity of k, separate discussions are given accordingly.

(1) *k* is an even number

When $s < -\lambda$, $(\lambda + s)^{k-1}$ is negative because k is an even number, and $(k+1)s + \lambda$ is negative owing to the positive value of k. Therefore, $f'(s)$ is positive. This means that when $s < -\lambda$, the curve of the function monotonically increases.

When s is negative infinity, the function will become

$$\lim_{s\to-\infty} f(s) = \lim_{s\to-\infty} s(\lambda + s)^{k} + \alpha\lambda^{k} = -\infty \qquad 3\text{-}29$$

Thus, when k is an even number, the curve of $f(s)$ can be roughly plotted as Fig. 2.

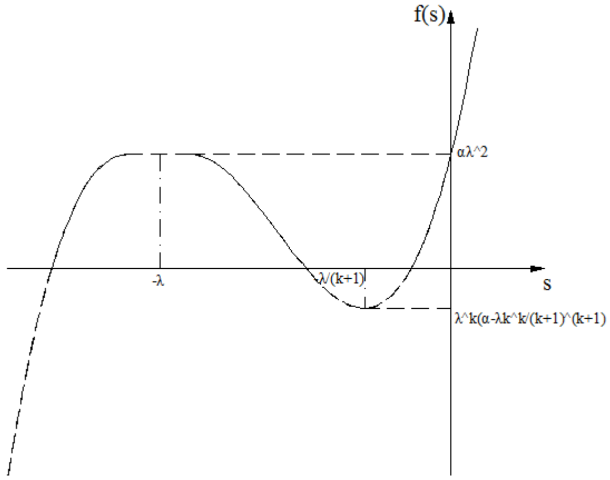

Fig. 2. The graph of $f(s)$ when k is even.

As demonstrated in **Fig. 2**, there is always a real root less than $-\lambda$. In addition, the other roots that are real or imaginary depend on the value of $f\left(-\frac{\lambda}{k+1}\right)$.

When $f\left(-\frac{\lambda}{k+1}\right) = \lambda^k \left(\alpha - \frac{k^k}{(k+1)^{k+1}}\lambda\right) < 0$, namely, $\alpha < \frac{k^k}{(k+1)^{k+1}}\lambda$, the equation has three real roots, and the maximum real root, which is dominated, is less than 0 and greater than $-\frac{\lambda}{k+1}$. We can conclude that the spacing between the lead and following vehicles is non-oscillatory on the basis of the characteristics of the roots.

When $f\left(-\frac{\lambda}{k+1}\right) = \lambda^k \left(\alpha - \frac{k^k}{(k+1)^{k+1}}\lambda\right) = 0$, namely, $\alpha = \frac{k^k}{(k+1)^{k+1}}\lambda$, the equation also has three real roots, but two repeated roots, and the maximum real root is $-\frac{\lambda}{k+1}$, which is dominated. Thus, the spacing between the lead and following vehicles remains stable.

When $f\left(-\frac{\lambda}{k+1}\right) = \lambda^k \left(\alpha - \frac{k^k}{(k+1)^{k+1}}\lambda\right) > 0$, namely, $\alpha > \frac{k^k}{(k+1)^{k+1}}\lambda$, there is only one real root. Two imaginary roots become dominated, and the headway trends toward oscillation.

(2) k is an odd number

Likewise, when $s < -\lambda$, $(\lambda + s)^{k-1}$ is positive because k is odd, and $(k+1)s + \lambda$ is still negative because of the positive value of k $f'(s)$ is negative. It means that when $s < -\lambda$, the curve of the function decreases monotonically.

When s is negative infinity, the function will become

$$\lim_{s \to -\infty} f(s) = \lim_{s \to -\infty} s(\lambda + s)^k + \alpha\lambda^k = +\infty. \qquad 3\text{-}30$$

Thus, the curve of $f(s)$ can be roughly plotted as **Fig. 3**.

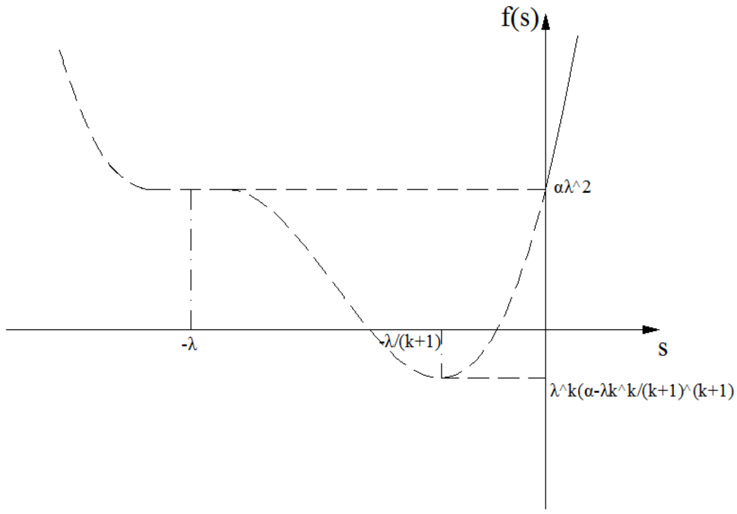

Fig. 3. The graph of $f(s)$ when k is odd.

The two roots are likely influenced by the minimum point $f\left(-\frac{\lambda}{k+1}\right)$. Similarly, we have the classified discussion.

When $f\left(-\frac{\lambda}{k+1}\right) = \lambda^k\left(\alpha - \frac{k^k}{(k+1)^{k+1}}\lambda\right) < 0$, namely, $\alpha < \frac{k^k}{(k+1)^{k+1}}\lambda$, there are two negative real roots. The spacing between the lead and following vehicles is non-oscillatory.

When $f\left(-\frac{\lambda}{k+1}\right) = \lambda^k\left(\alpha - \frac{k^k}{(k+1)^{k+1}}\lambda\right) = 0$, namely, $\alpha = \frac{k^k}{(k+1)^{k+1}}\lambda$, the equation has two repeated real roots. The headway is still stable.

When $f\left(-\frac{\lambda}{k+1}\right) = \lambda^k\left(\alpha - \frac{k^k}{(k+1)^{k+1}}\lambda\right) > 0$, namely, $\alpha > \frac{k^k}{(k+1)^{k+1}}\lambda$, there are two imaginary roots. The spacing between the two vehicles is oscillatory with increasing amplitude.

In conclusion, whether k is even or odd, the demarcation point of stability is $C = \alpha\frac{k}{\lambda} = (\frac{k}{k+1})^{k+1}$. When $C \leq (\frac{k}{k+1})^{k+1}$, the spacing between the lead and following vehicles remains stable. When $C > (\frac{k}{k+1})^{k+1}$, the headway between the two vehicles is oscillatory. In addition, as the value of k in the gamma distribution increases, the stability point approaches 1/e=0.367879, which is the critical point as calculated by Herman et al. (1959).

To summarize, according to the results of the stability point as $\alpha = \frac{k^k}{(k+1)^{k+1}}\lambda$, and the undamped point as $\alpha = k * \frac{\sin(k\theta)\cdot\sin\theta}{(cos\theta)^{k+1}}$, a series of pairs of points with different values for k is calculated in **Table 2**.

Table 2. Stability and undamped points with different values of *k*.

k	2	3	4	5	6	7	8	9	10	11	12
Stability point	0.2963	0.3164	0.3277	0.3349	0.3399	0.3436	0.3464	0.3487	0.3505	0.3520	0.3533
Undamped point	4.0000	2.6667	2.2742	2.0879	1.9794	1.9085	1.8585	1.8214	1.7927	1.7699	1.7514

The following figure presents the stable and unstable regions with respect to k.

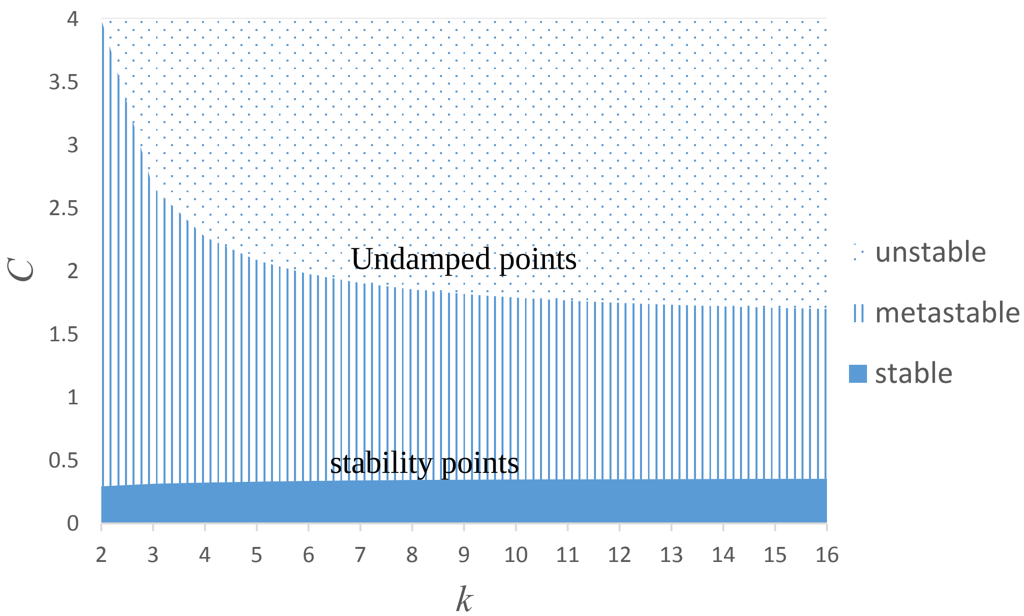

Fig. 4. Regions demarcated by stability and undamped points.

The space has been divided into three regions by the stability and undamped points. The minimal zone below the line of the stability points is the stable region, which signifies that the spacing is non-oscillatory. The intermediate region is a metastable region, indicating that the headway has a trend toward oscillation but finally stabilizes. Above the line of undamped points is the unstable region, which indicates that the amplitude of the oscillation will strictly increase and never fade away, that the system is unstable, and that a collision will definitely occur.

Fig. 4 illustrates the enlargement of the metastable region of damped oscillation by taking into account the driver's memory effect, in contrast to the approach of the traditional car-following model. Meanwhile, the stable region is slightly reduced, which means that the local stability, with respect to the stability and metastability situation, of the car-following system is improved by the introduction of the memory effect.

4 NUMERICAL STUDY

In this section, a numerical example is presented for stability analysis on the basis of the car-following model with a stochastic memory effect.

4.1 Numerical example

In a car-following system, the lead and following vehicles are both presumed to begin traveling at a speed of 10 m/s with spacing of 10 m. Therefore, $x_n(0) = 0$, $x_{n+1}(0) = -10$, $\dot{x}_n(0) = 10$, and $\dot{x}_{n+1}(0) = 10$. The lead vehicle first decelerates and then accelerates according to the speed trajectory shown in **Fig. 5**.

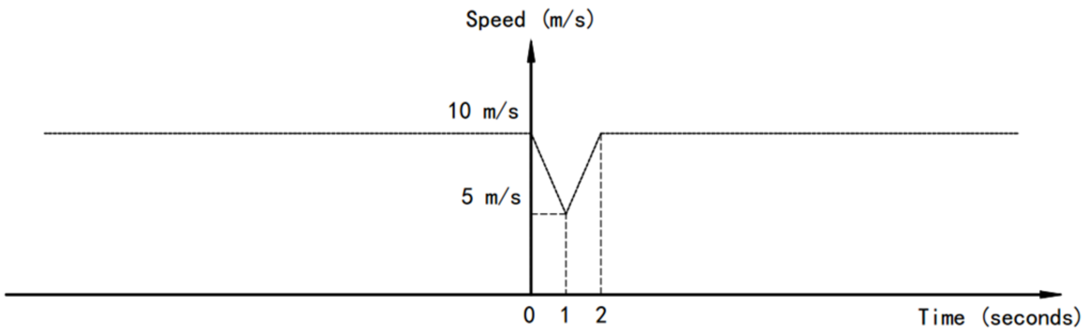

Fig. 5. Speed trajectory of the lead vehicles.

In practice, on the basis of the memory effect car-following model

$$\ddot{x}_{n+1}(t) = \alpha \int_0^{+\infty} f(\omega)(\dot{x}_n(t-\omega) - \dot{x}_{n+1}(t-\omega))d\omega,$$

we simplify the integration as the summation of the memory effects of relative velocity at each moment during 0 to T with time step $\tau = 0.1s$. The acceleration of the following car should be estimated as

$$\ddot{x}_{n+1}(t) = \alpha \sum_{m=0}^{T/\tau} f(m\tau)(\dot{x}_n(t-m\tau) - \dot{x}_{n+1}(t-m\tau))\,\tau. \qquad \text{4-1}$$

Furthermore, the spacing of the two vehicles should be calculated according the speed and acceleration of each vehicle, which is used to monitor the stability of the supposed car-following system.

In light of the previous empirical study, the memory effect period T is less than 10 s; above this value, the probability of a gamma distribution is less than 0.01.

4.2 Stability analysis and simulation

As a preliminary analysis, we assume that $k = \lambda = 10$; ; , then, ; the mean of the gamma distribution is then $\mathrm{E}(\omega) = k/\lambda = 1$, and the variance is $\mathrm{D}(\omega) = k/\lambda^2 = 0.1$. Thus, $C = \alpha\frac{k}{\lambda} = \alpha$ in this case. The value of the sensitivity factor determines the stability of the supposed car-following system. The undamped and stability points are discussed and compared with the analytical results for different values of α.

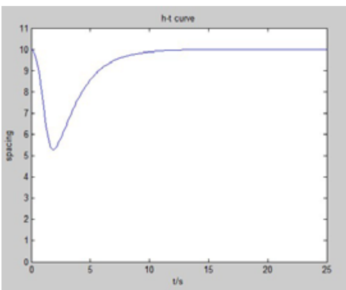

a) $C = \alpha = 0.30$

No oscillation

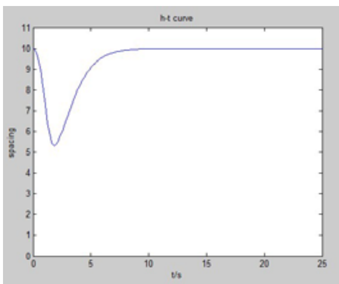

b) $C = \alpha = 0.35$

Stability point

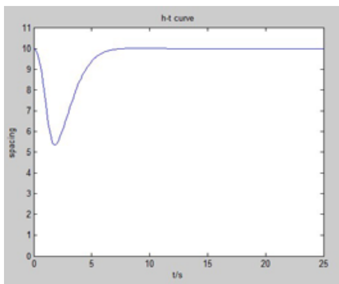

c) $C = \alpha = 0.40$

Damped oscillation

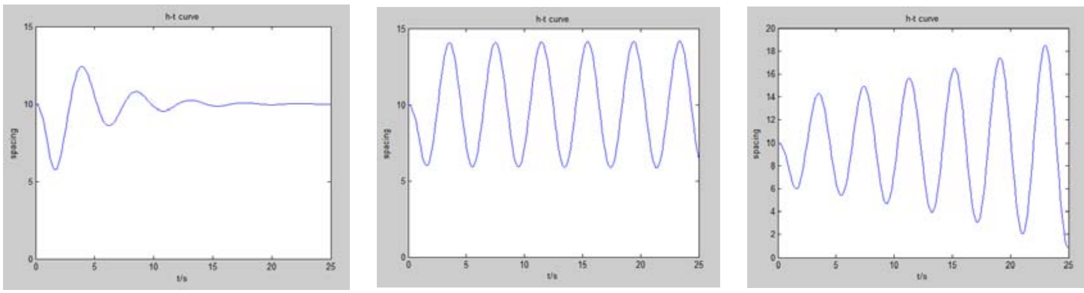

d) $C = \alpha = 1.20$ *Damped oscillation*

e) $C = \alpha = 1.80$ *Undamped point*

f) $C = \alpha = 1.90$ *Amplifying oscillation*

Fig. 6. Stability analysis and simulation.

According to the results of the simulation as shown in **Fig. 6**, the stability point should be around 0.35 and the undamped point around 1.80, which are consistent with the analytical results, with corresponding points of 0.3505 and 1.7927, respectively.

Furthermore, the stability analysis was performed for different gamma distribution profiles with different values for k and λ.

First, the mean of the gamma distribution is kept constant, i.e. $\mathrm{E}(\omega) = k/\lambda = 1$, whereas a standard deviation of σ would be different. We obtain the undamped and stability points as shown in **Table 3**.

Table 3. Stability comparison of the analytical and numerical studies with the same mean.

k	λ	σ	Stability point		Undamped point	
			numerical study	analytical study	numerical study	analytical study
2	2	0.500	0.332	0.2963	3.91	4.0000
3	3	0.333	0.330	0.3164	2.65	2.6667
4	4	0.250	0.334	0.3277	2.27	2.2742
5	5	0.200	0.338	0.3349	2.09	2.0879
6	6	0.167	0.342	0.3399	1.98	1.9794
7	7	0.143	0.345	0.3436	1.91	1.9085
8	8	0.125	0.348	0.3464	1.86	1.8585
9	9	0.111	0.350	0.3487	1.82	1.8214
10	10	0.100	0.352	0.3505	1.79	1.7927

11	11	0.091	0.353	0.3520	1.77	1.7699
12	12	0.083	0.355	0.3533	1.75	1.7514

The results of the simulation are consistent with those of the previous analytical study. We plot the curves of the stability and undamped points, respectively, for further demonstration.

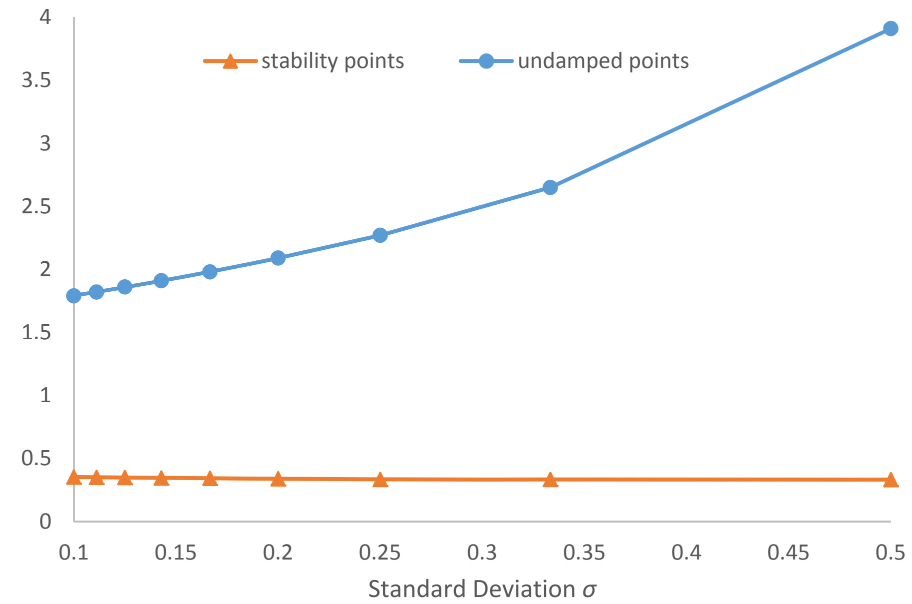

Fig. 7. Critical points for different variance.

As shown in **Fig. 7**, when the variance of the gamma distribution was smaller, the stability point was closer to 1/e (≈ 0.367879). Meanwhile, when the variance was smaller, the undamped point was closer to $2/\pi$ (≈ 1.57). In special cases in which the variance is zero, the memory effect model reduces to the traditional model with a fixed time lag. The results of critical point calculation are therefore consistent with those of the traditional car-following model found by Herman (1959). In addition, we notice that all of the stability points with a stochastic time lag are less than 1/e (≈ 0.367879), whereas the undamped points are more than $2/\pi$ (≈ 1.57), which means that the incorporation of the driver's memory effect weakens the stable region but reduces the chances of instability or collision.

We also see in **Fig. 7** that the stability point slightly decreases with an increase in the standard deviation, whereas the undamped point increases. This finding indicates that it would be slightly more difficult to obtain stability in a following driver with a wide range of more effective memory of relative velocities; however, such a driver would be less likely to suffer instability or collision. This conclusion is reasonable because a driver with good memory should be thoughtful and make decisions on the basis of greater experience and past information, which is generally beneficial in terms of car-following behavior.

The variance of the gamma distribution is then maintained as a constant, i.e., $\mathrm{D}(\omega) = k/\lambda^2 = 0.1$. We obtain the undamped and stability points as shown in Table 4.

Table 4. Stability comparison of the analytical and numerical studies with same variance.

k	λ	$\mathrm{E}(\omega)$	Stability point		Undamped point	
			numerical study	analytical study	numerical study	analytical study
2	4.5	0.447	0.300	0.2963	3.77	4.0000
3	5.5	0.548	0.318	0.3164	2.66	2.6667
4	6.3	0.632	0.328	0.3277	2.28	2.2742
5	7.1	0.707	0.336	0.3349	2.09	2.0879
6	7.7	0.775	0.341	0.3399	1.98	1.9794
7	8.4	0.837	0.345	0.3436	1.92	1.9085
8	8.9	0.894	0.347	0.3464	1.86	1.8585
9	9.5	0.949	0.350	0.3487	1.82	1.8214
10	10.0	1.000	0.352	0.3505	1.79	1.7927
11	10.5	1.049	0.353	0.3520	1.77	1.7699
12	11.0	1.095	0.354	0.3533	1.75	1.7514

As a result, the simulated critical points are consistent with the results of the analytical study. We also plot the curves of the stability and undamped points as shown in **Fig. 8**. With an increase in the mean of the time lag, the stability point slightly increases, whereas the undamped point decreases. As in the traditional car-following model, a longer time lag increases the likelihood of an unstable situation or a collision.

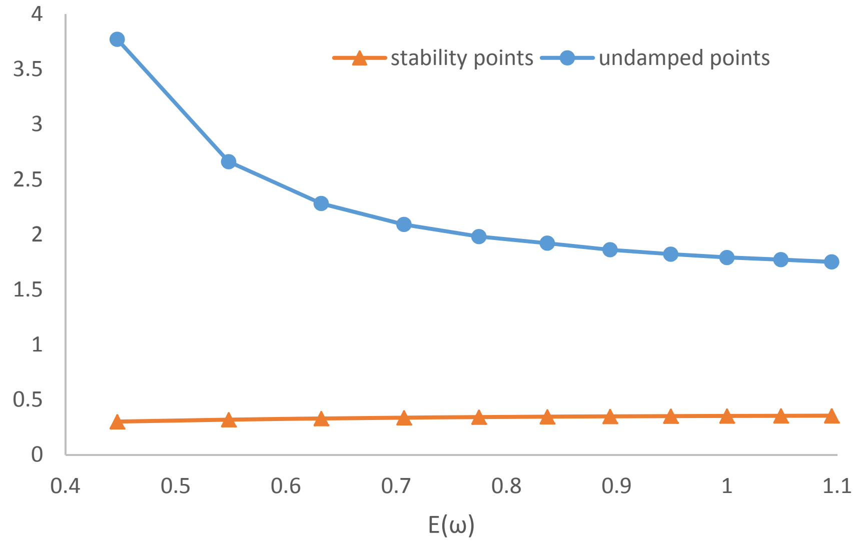

Fig. 8. Critical points for different means.

5 CONCLUSIONS

A car-following model with a stochastic memory effect is considered to be more realistic in modeling drivers' behavior. In this study, we first identified the gamma distribution as the optimal form of memory function according to the empirical data. Analytical and numerical studies are conducted for the stability analysis of the gamma-distributed memory effect of the car-following model.

On the basis of the transfer function from the Laplace transform, the general expression of the undamped and stability points is solved in the analytical study. The results indicate that the stability points slightly decrease by introduction of the driver's memory effect, whereas the undamped points obviously increase, which agrees well with the results of the numerical study. The conclusion therefore is that the rigid local stability will not be improved if the driver comprehensively considers the past information, but he or she would have a better chance of handling the spacing to avoid any collisions. In addition, the stable and unstable regions with respect to the different profiles of the gamma distribution are found to be different. An agile and thoughtful driver with a good memory in terms of a smaller mean and a wide variance would be less likely to fall into the unstable region.

Because existing studies focus only on the linear model with a memory effect, it would be worthwhile for a future study to extend the analysis to a nonlinear memory effect model. We also would like to verify the stability points on the basis of empirical data. Furthermore, the parameter of memory function and the sensitivity factor may vary among different drivers over time, which is also an interesting topic that would help to monitor car-following behavior for safe driving.

ACKNOWLEDGEMENTS

The work described in this paper was supported by grants from the National Natural Science Foundation of China (Grant No. 71301083), the National Basic Research Program of China (973 Project; No.2012CB725405), the Research Funds of Tsinghua University (No. 20151080412), the Research Grants Council of the Hong Kong Special Administrative Region, China (Project Nos. 718811 and 717512), and the National Research Foundation of Korea funded by the Korean Government (MEST) (NO. NRF-2010-0029446). We would like to thank Prof. Wang Jianqiang from Tsinghua University for conducting the car-following experiments and providing the experimental data for our empirical analysis.

REFERENCES

Andrews D.W.K. and Buchinsky M. (2000) A three-step method for choosing the number of bootstrap repetitions. *Econometrica*, **68**(1), 13-51.

Bando M., Hasebe K., Nakayama A., Shibata A., and Sugiyama Y. (1995) Dynamical model of traffic congestion and numerical simulation. *Physical Review E*, **51**, 1035.

Cao B. (2015) A new car-following model considering driver's sensory memory. *Physica A*, **427**, 218-225.

Chandler R.E., Herman R., and Montroll E.W. (1958) Traffic dynamics: studies in car following. *Operations Research,* **6**(2), 165-184.

Gazis D.C., Herman R., and Rothery R.W. (1961) Non-linear follow the leader models of traffic flow. *Operations Research*, **9**, 545-567.

Ge H.X., Meng X.P., Ma J., and Lo S.M. (2012) An improved car-following model considering influence of other factors on traffic jam. *Physics Letters A*, **377**(1-2), 9-12.

Herman R., Montroll E.W., Potts R.B., and Rothery R.W. (1959) Traffic dynamics: analysis of stability in car-following. *Operations Research,* **7**(1), 86-106.

Jiang R., Wu Q., and Zhu Z. (2001) Full velocity difference model for a car-following theory. *Physical Review E*, **64**, 017101.

Jin, I. G., Orosz, G. (2014) Dynamics of connected vehicle systems with delayed acceleration feedback. *Transportation Research Part C*, **46** (9), 46-64.

Kesting, A. and Treiber, M. (2008) How reaction time, update time, and adaptation time influence the stability of traffic flow. *Comput Aided Civil Infrastruct Eng*, **23**, 125-137.

Lee G. (1966) A generalization of linear car-following theory. *Operations Research* **14**(4), 595-606.

Monteil, J., Billot, R., Sau, J., El Faouzi, N.-E., (2014) Linear and weakly nonlinear stability analyses of cooperative car-following models. *IEEE Transactions on Intelligent Transportation Systems*, **15**, 2001-2013.

Newell G.F. (1961) Nonlinear effects in the dynamics of car following. *Operations Research*, **9**(2), 209-229.

Ngoduy, D (2013) Analytical studies on the instabilities of heterogeneous intelligent traffic flow. *Communications in Nonlinear Science and Numerical Simulation*, **18** (10), 2699-2706

Ngoduy, D (2015) Linear stability of a generalized multi-anticipative car following model with time delays. *Communications in Nonlinear Science and Numerical Simulation*, **22**, 420-426

Pipes L.A. (1953) An operational analysis of traffic dynamics. *Journal of Applied Physics*, **24**, 271-281.

Reuschel A. (1950) Fahrzeugbewegungen in der Kolonne Beigleichformig beschleunigtem oder vertzogerten Leitfahrzeub, Zeit. D. Oster. Ing. U. Architekt Vereines Ed. (Vehicle Movements in a Platoon with Uniform Acceleration or Deceleration of the Lead Vehicle), 50-62 and 73-77.

Sipahi R., Atay F.M., Niculescu S.H. (2007) Stability of traffic flow behavior with distributed delays modeling the memory effects of the drivers. *SIAM Journal on Applied Mathmatics,* **68**(3), 738-759.

Tang T.Q., Huang H.J., Zhao S.G., and Xu G. (2009) An extended OV model with consideration of driver’s memory. *International Journal of Modern Physics B*, **23**(5), 743-752.

Tang T.Q., Li C.Y., Huang H.J. (2010) A new car-following model with the consideration of the driver's forecast effect. *Physics Letters A*, **374**(38), 3951-3956.

Treiber, M., and Helbing, D. (2003). Memory effects in microscopic traffic models and wide scattering in flow-density data. *Physical Review E*, **68**(4), 046119.

Treiber, M., Kesting, A. and Helbing, D. (2006). Delays, inaccuracies and anticipation in microscopic traffic model. *Physica A*, **360**, 71-88.

Xin Z. and Xu J. (2015) Analysis of a Car-Following Model with Driver Memory Effect. *International Journal of Bifurcation and Chaos*, **25**(4), 1550037.

Yu S. and Shi Z. (2015a) An improved car-following model considering headway changes with memory. *Physica A*, **421**, 1-14.

Yu S. and Shi Z. (2015b) The effects of vehicular gap changes with memory on traffic flow in cooperative adaptive cruise control strategy. *Physica A*, **428**, 206-223.

Zhang, HM (2003) Driver memory, traffic viscosity and a viscous vehicular traffic flow model. *Transportation Research Part B*, **37** (1), 27-41.